Electronic Supplementary Material

MoS_2-wrapped silicon nanowires for photoelectrochemical water reduction

Liming Zhang[1,†,§], Chong Liu[1,§], Andrew Barnabas Wong[1,4], Joaquin Resasco[2], and Peidong Yang[1,3,4] (✉)

[1] *Department of Chemistry, University of California, Berkeley, CA 94720, USA*
[2] *Department of Chemical Engineering, University of California, Berkeley, CA 94720, USA*
[3] *Department of Materials Science and Engineering, University of California, Berkeley, CA 94720, USA*
[4] *Materials Science Division, Lawrence Berkeley National Laboratory, Berkeley, CA 94720, USA*
[†] *Present address: Department of Materials Science and Engineering, Stanford University, Stanford, CA 94305, USA*
[§] *These authors contributed equally to this work.*

Supporting information to DOI 10.1007/s12274-014-0673-y

Nanowire (NW) array synthesis: The well-defined periodic silicon (Si) NW arrays (Figs. 3(c) and 3(d)) were fabricated using reactive-ion etching of patterned single-crystalline Si wafers. P-type boron-doped 4′′ Si wafers (<100> oriented, 0.1–0.2 Ω·cm) were first patterned with a photoresist dot array using a standard photolithography stepper. Then the wafer underwent inductive-coupled plasma deep reactive-ion etching (Surface Technology Systems, Inc.) to produce NW arrays with uniform diameter ~850 nm and length ~30 μm. After removing the residual photoresist by an O_2 plasma, 50 nm of dry thermal oxide was grown on the NWs at 1,050 °C for 40 min. After a 5:1 buffered HF etch and critical point drying (Tousimis, Inc.), Si NW arrays with wires whose diameters were about 800 nm were obtained.

Atomic layer deposition (ALD) of TiO_2: The deposition procedure was developed based on the previous reported method [S1]. Si NWs array samples were etched in 1:10 HF buffer solution for 1 min, and cleaned with DI water and isopropyl alcohol, followed by rapid drying on a hot plate at a temperature of 90 °C. This fast drying method helps to maintain the vertical morphology of NW array. TiO_2 shells were deposited on Si NW array by using a custom built ALD system at 300 °C with $TiCl_4$ (99.99%, Alfa) and pure DI water as the precursors. The deposition rate was ~0.5 Å/cycle.

Low temperature annealing of MoS_2: The MoS_2 cocatalyst was synthesized on the surface of NWs by thermal annealing of molybdenum precursor, $(NH_4)_2MoS_4$, under reducing atmosphere. $(NH_4)_2MoS_4$ powder (Alfa Asear, purity of 99.99%, 0.125 g) was dissolved into methanol/hexamethyldisilazane (HMDS) solution (10 mL/20 μL) under magnetic agitation to fully disperse the powder. The low surface tension solvent HMDS (18.2 mN/m at 293 K) was used to preserve the morphology of the NW array. The solution was drop-casted onto the NW surface. The drop-casting volume depends on the density (roughness factor) of the NW array and the projected area of Si substrate. For example, for a 1 cm × 1 cm Si substrate with a NW array with surface roughness factor 30, the optimal volume was 25 μL. A glass dish cap was used to cover the substrate to allow for slow evaporation

---

Address correspondence to p_yang@berkeley.edu

of the methanol. MoS_2 layers were obtained by annealing the precursor at 300–400 °C in a N_2/H_2 (80/20 sccm) atmosphere at ambient pressure for 2 h.

Transmission electron microscopy (TEM): Electron microscopy was performed at the National Center for Electron Microscopy in Lawrence Berkeley National Lab. TEM images were taken at 200 kV on a FEI Tecnai F20 microscope with an ultra-twin lens. High-angle annular dark-field (HAADF) images and energy dispersive X-ray spectroscopy (EDS) maps were acquired using a FEI Titan microscope operated at 80 kV. The microscope was equipped with a Fischione HAADF detector that had inner semi-angle of 79 mrad. EDS mapping images were acquired using a FEI Super-X Quad windowless detector based on silicon drift technology and processed using Bruker Esprit software, which was calibrated against mineral standards for quantitative accuracy.

X-ray photoelectron spectroscopy (XPS) and Raman spectroscopy: XPS spectra were collected using a PHI 5400 X-ray Photoelectron Spectrometer equipped with a 4 kV Argon ion gun, with Al Kα radiation. The angle between the source and detector was 35°. The measurement chamber was maintained at 10^{-9} eV during measurement, and measurements were taken at a pass energy of 17.9 eV. All energies were calibrated to adventitious carbon at 285.0 eV. Raman spectroscopy was taken by a Horiba HR800 system with laser excitation energy of 532 nm. The laser spot size is ~1 μm and a laser power of ~5 mW was used to avoid heating.

Photoelectrochemistry (PEC) measurements: Electrochemical and photoelectrochemical measurements of electrodes were performed using a Biologic potentiostat. All measurements were performed under purged Ar gas environment and in a 0.5 M sulfuric acid electrolyte (pH = 0.48). Ag/AgCl in 1 M NaCl (CHI, Corp.) was used as a reference electrode when needed, and all voltages reported were calculated versus the reversible hydrogen electrode (RHE) using the following equation

$$V \text{ vs. RHE (volt)} = V \text{ vs. Ag/AgCl (volt)} + 0.234 \text{ (volt)} + 0.0591 \times \text{pH}$$

The light source used for simulated sunlight in this report was a 300 W xenon lamp equipped with an air mass 1.5 G filter (Newport). Before each measurement, a calibrated silicon photodiode determined the light intensity at the position of the electrode being measured. The J–V photocurrent data for individual photoelectrodes were measured using a standard three-electrode setup under simulated one-sun illumination, with a scan rate of 10 mV/sec. The dark currents were orders of magnitude lower than photocurrent in all cases within the voltage ranges measured. For the incident photon to current conversion efficiency (IPCE) measurement, a 300 W Xe lamp was coupled with a monochromator (Newport, Cornerstone 130), and the incident light intensity was measured with a calibrated Si photodiode. Here, the IPCE was calculated from the photocurrents measured at –0.33 V vs. RHE, according to the following equation

$$\text{IPCE} = \frac{I_{\text{ph}}\left(\dfrac{\text{mA}}{\text{cm}^2}\right) \times 1239.8(\text{V}\cdot\text{nm})}{P_{\text{mono}}\left(\dfrac{\text{mW}}{\text{cm}^2}\right) \times \lambda(\text{nm})}$$

Determination of faradaic efficiency: The experiment was conducted in a sealed cell containing 0.5 M H_2SO_4 electrolyte through which Ar carrier gas was flowed at a rate of 5 sccm. Controlled potential electrolysis were conducted at an applied potential of –0.33 V vs. RHE for 75 min. Figure S5 shows the generated hydrogen volume during photoelectrolysis in sulfuric acid based on a gas chromatography (Varian Micro-GC with a Molecular Sieve 5 Å column, 40 m) measurement.

Table S1 Calculation of the electrochemical performance of MoS_2

Precursor loading volume (μL)	MoS_2 loading amount[a] (10^{-7} mol/cm^2)	j_0[b](10^{-8}A/cm^2)	Tafel slope[c] (mV/dec)
1.0	0.48	2.62 ± 0.12	74.7 ± 0.4
2.5	1.2	4.15 ± 0.14	74.8 ± 0.3
5.0	2.4	8.97 ± 0.21	78.6 ± 0.3
10	4.8	23.6 ± 0.7	84.2 ± 0.5

[a] The absolute loading amount of MoS_2 is calculated based on the concentration and loading volume of precursor.

[b] j_0 exchange current density and [c]Tafel slope were calculated from Tafel plots in Fig. 3(b).

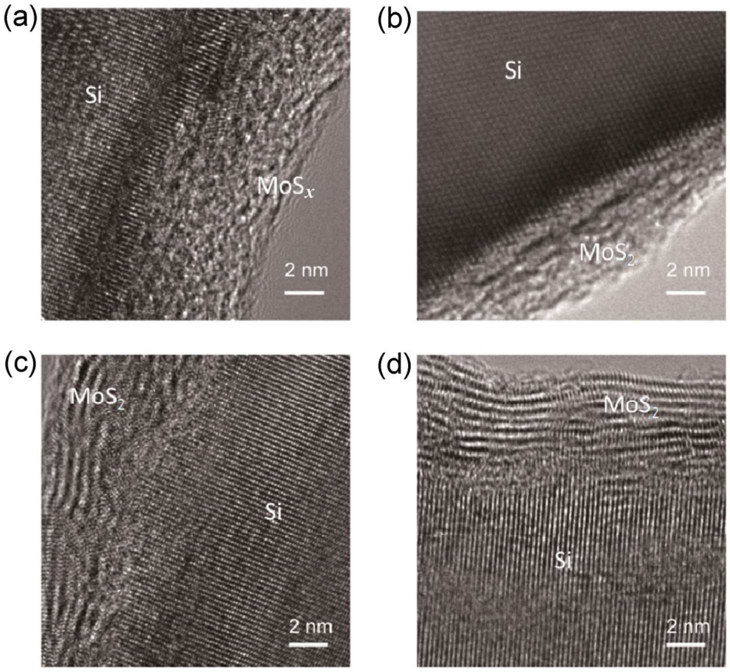

Figure S1 High-resolution TEM images of MoS_x on NW (a) without annealing and at different annealing temperatures of (b) 200 °C, (c) 300 °C, and (d) 400 °C. The crystallinity of MoS_2 highly depends on the annealing temperature, with increasing temperature resulting in higher crystallinity.

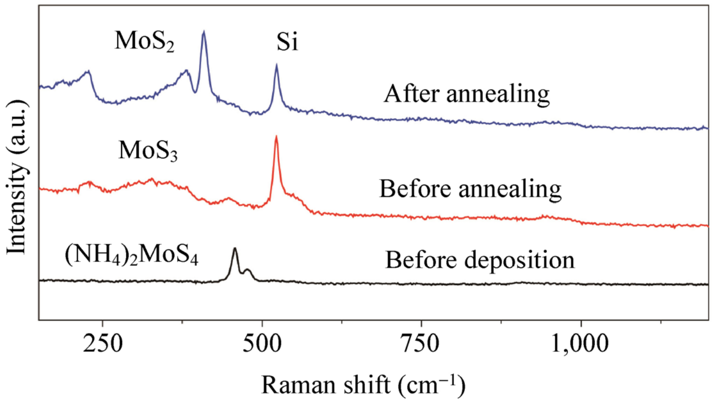

Figure S2 Raman spectra evolution of cocatalysts before and after thermal annealing. The peaks at ~383 and 407 cm^{-1} demonstrate the formation of MoS_2.

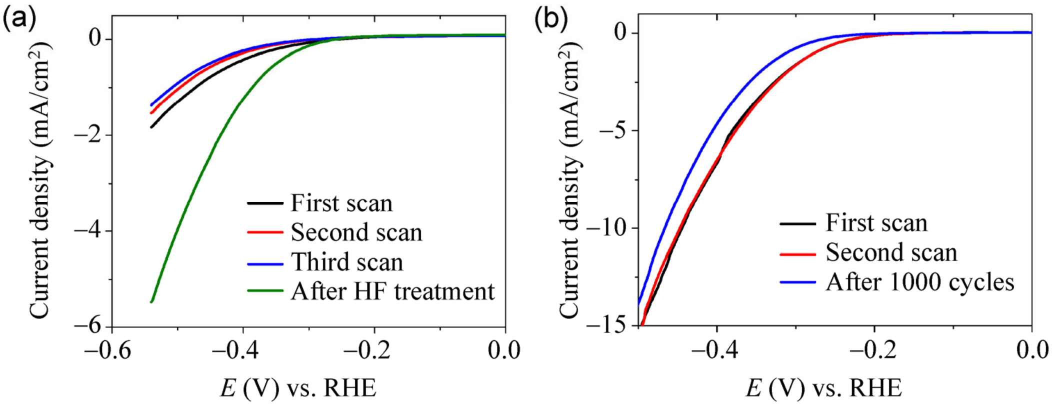

Figure S3 Linear sweep voltammograms for (a) p^+Si and (b) TiO_2/p^+ Si planar surface coated with MoS_2 cocatalyst. The performance recovery after HF treatment in (a) indicates the oxidation of Si is the main cause for the performance degradation.

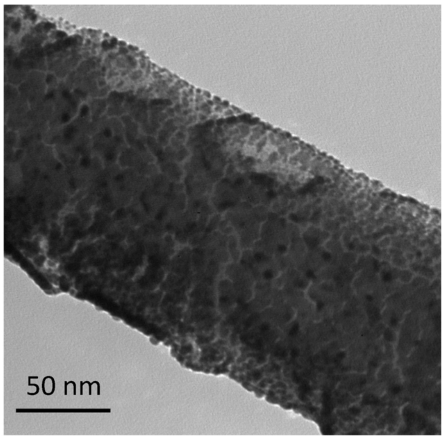

Figure S4 TEM image of a Pt nanoparticle coated TiO_2/Si NW.

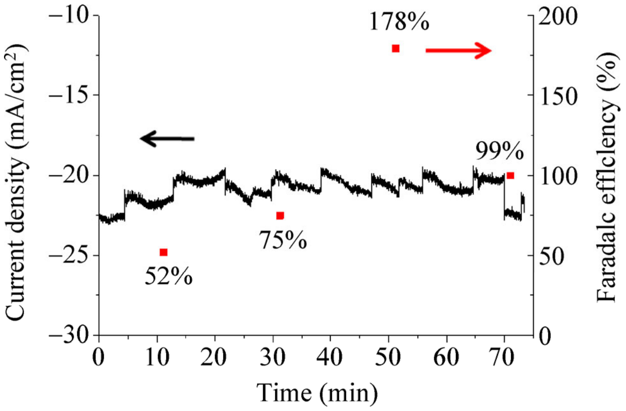

Figure S5 Chronoamperometry measurement of $MoS_2/TiO_2/n^+p$-Si NW array held at a constant potential of –0.33 V vs. RHE under 1 sun illumination. Bubbles were continuously evolved from photocathode, and the accumulation and release of these bubbles led to the observed variations in photocurrent over the duration of the measurement. The large variation of faradaic efficiency originated from the accumulation of hydrogen bubble on the electrode surface. The average faradaic efficiency calculated in the 75 min time range is ~100%.

Reference

[S1] Hwang, Y. J.; Hahn, C.; Liu, B.; Yang, P. *ACS Nano* **2012**, *6*, 5060.